

Article

Evidence of Unknown Paleo-Tsunami Events along the Alas Strait, West Sumbawa, Indonesia

Bachtiar W. Mutaqin ^{1,2,*}, Franck Lavigne ^{2,*}, Patrick Wassmer ^{2,3}, Martine Trautmann ³,
Puncak Joyontono ¹, Christopher Gomez ⁴, Bagus Septiangga ⁵, Jean-Christophe Komorowski ⁶,
Junun Sartohadi ⁷ and Danang Sri Hadmoko ¹

- ¹ Coastal and Watershed Research Group, Faculty of Geography, Universitas Gadjah Mada, Yogyakarta 55281, Indonesia; puncak.joyontono@mail.ugm.ac.id (P.J.); hadmoko@ugm.ac.id (D.S.H.)
 - ² Laboratoire de Géographie Physique, Université Paris 1 Panthéon Sorbonne, 75231 Paris, France; wassmerpat@aol.com
 - ³ Faculté de Géographie et d'Aménagement, Université de Strasbourg, 67000 Strasbourg, France; martine.trautmann@unistra.fr
 - ⁴ Department of Maritime Sciences, Graduate School of Maritime Sciences, Kobe University, Kobe, Hyogo 657-8501, Japan; christophergomez@bear.kobe-u.ac.jp
 - ⁵ Directorate General of Water Resources, Ministry of Public Works and Housing, Jakarta 12110, Indonesia; septianggabagus@gmail.com
 - ⁶ Institut de Physique du Globe de Paris UMR 7154, Université Sorbonne Paris Cité, 75005 Paris, France; komorow@ipgp.fr
 - ⁷ Faculty of Agriculture, Universitas Gadjah Mada, Yogyakarta 55281, Indonesia; junun@ugm.ac.id
- * Correspondence: mutaqin@ugm.ac.id (B.W.M.); franck.lavigne@univ-paris1.fr (F.L.)



Citation: Mutaqin, B.W.; Lavigne, F.; Wassmer, P.; Trautmann, M.; Joyontono, P.; Gomez, C.; Septiangga, B.; Komorowski, J.-C.; Sartohadi, J.; Hadmoko, D.S. Evidence of Unknown Paleo-Tsunami Events along the Alas Strait, West Sumbawa, Indonesia. *Geosciences* **2021**, *11*, 46. <https://doi.org/10.3390/geosciences11020046>

Received: 23 October 2020
Accepted: 20 January 2021
Published: 23 January 2021

Publisher's Note: MDPI stays neutral with regard to jurisdictional claims in published maps and institutional affiliations.



Copyright: © 2021 by the authors. Licensee MDPI, Basel, Switzerland. This article is an open access article distributed under the terms and conditions of the Creative Commons Attribution (CC BY) license (<https://creativecommons.org/licenses/by/4.0/>).

Abstract: Indonesia is exposed to earthquakes, volcanic activities, and associated tsunamis. This is particularly the case for Lombok and Sumbawa Islands in West Nusa Tenggara, where evidence of tsunamis is frequently observed in its coastal sedimentary record. If the 1815 CE Tambora eruption on Sumbawa Island generated a tsunami with well-identified traces on the surrounding islands, little is known about the consequences of the 1257 CE tremendous eruption of Samalas on the neighboring islands, and especially about the possible tsunamis generated in reason of a paucity of research on coastal sedimentary records in this area. However, on Lombok Island, the eruption of the Samalas volcano produced significant volumes of pyroclastic flows that entered the sea in the North and East of the island. These phenomena must have produced a tsunami that left their traces, especially on Sumbawa Island, whose western coastline is only 14 km away from Lombok's eastern shore. Therefore, the main goal of this study is to investigate, find evidence, and determine the age of marine-origin sediments along the shore of the Alas Strait, Indonesia. We collected and analyzed samples of coral and seashells from marine deposits identified along the west coast of Sumbawa, i.e., in Belang Island and abandoned fishponds in Kiantar Village, in order to identify the sources and the occurrence period of these deposits events. Based on the radiocarbon dating of coral and seashell samples, we concluded that none of the identified marine deposits along the western coast of Sumbawa could be related chronologically to the 1257 CE eruption of Samalas. However, possible tsunami deposits located in Belang Island and abandoned fishponds in Kiantar Village yielded 4th century CE, 9th century CE, and 17th century CE. We also conclude that past large earthquakes triggered these tsunamis since no known volcanic eruption occurred near the Alas Strait at that time that may have triggered a tsunami.

Keywords: paleo-tsunami; grain size; radiocarbon dating; wave direction; Lombok; Sumbawa; Indonesia

1. Introduction

The Indian Ocean earthquake and tsunami on 26 December 2004 is considered as a turning point of disaster awareness and mitigation, especially in Indonesia, since they

changed their disaster paradigm from response to preparation and damage prevention following that event. This event also highlighted the fact that earthquakes and tsunamis remain unpredictable natural hazards [1–4]. Due to its tectonic configuration, Indonesia is continuously exposed to earthquakes and volcanic activities, as well as their related hazards such as landslides and tsunamis [5–12]. This makes it a useful natural laboratory. According to the global historical tsunami database from National Geophysical Data Center—NOAA, since the 4th century, at least 180 tsunamis have occurred (questionable, probable, and definite tsunamis) in Indonesia [13].

As a result of plate tectonics subduction between the Australian Plate and the Eurasian Plate, Lombok and Sumbawa Island (Figure 1), located in the inner arc of the Lesser Sunda Islands, are at risk of earthquakes [11,14]. In 2018, Lombok Island was struck by a sequence of deadly earthquakes between 29 July and 19 August 2018 triggered by the Flores thrust close to the north coast of Lombok [15–18]. Furthermore, Lombok and Sumbawa Islands are the location of two volcanoes of whom their eruptions had global ramifications in the 13th and the 19th century, i.e., Samalas and Tambora volcanoes, respectively [11,12,19–24].

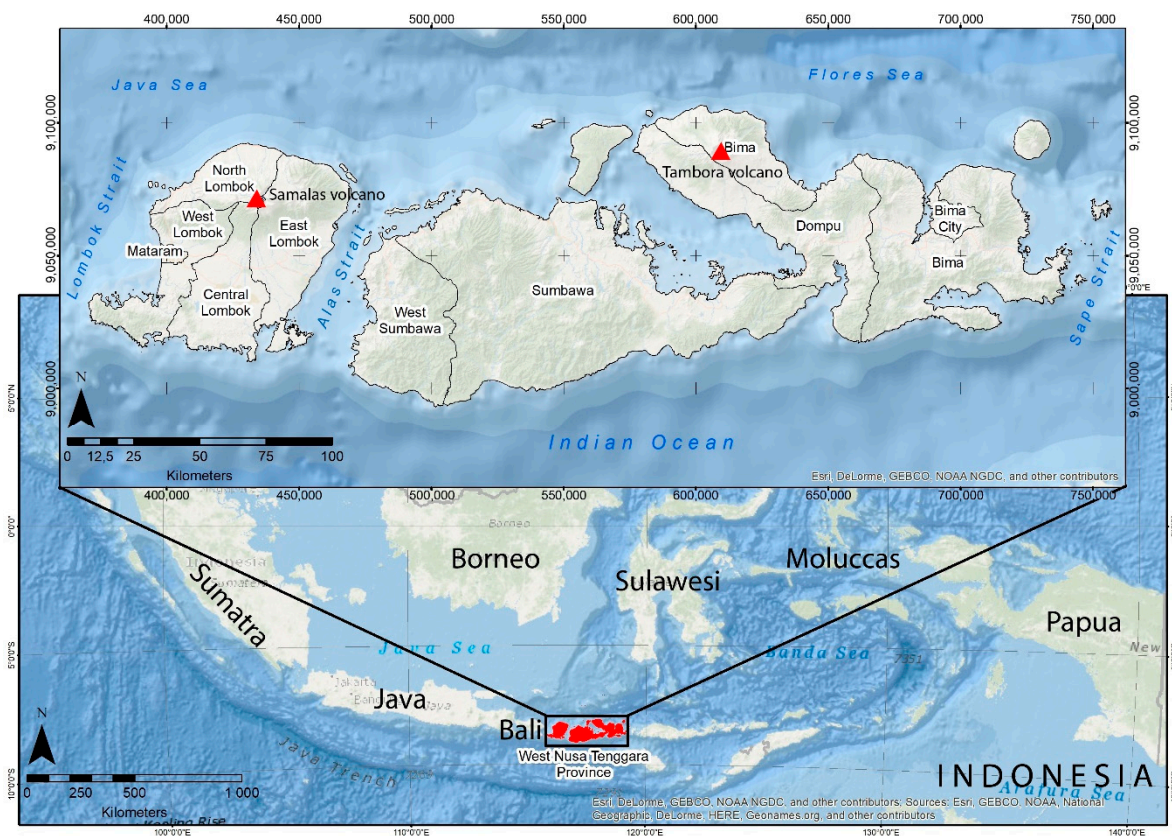


Figure 1. Lombok and Sumbawa Island in the inner arc of the Lesser Sunda Islands.

The 1815 CE eruption of the Tambora in Sumbawa triggered severe climate disturbances worldwide, earning the label “year without summer” in the Northeastern USA, Maritime Provinces of Canada, and Europe the year after the volcano erupted [25–29]. This eruption produced a total volume of about $41 \pm 4 \text{ km}^3$ dense rock equivalent (DRE) ($23 \pm 3 \text{ km}^3$ DRE ash fall and $18 \pm 6 \text{ km}^3$ DRE pyroclastic flows) [21]. The 1815 CE Tambora eruption also generated a tsunami with well-identified traces in Sumbawa Island [26]. Severe impacts were also felt by the world’s population and the global environment due to the 1257 CE Samalas eruption, which produced more than 40 km^3 DRE of volcanic deposits [30–33]. The impacts included famine and death in Europe due to climate anomalies, especially over Western Europe in 1258 [31,33]. Furthermore, the surface air temperature

and the sea surface temperature also decreased by about 1.6 °C and 0.8 °C, respectively, in response to the 1257 CE Samalas eruption [30].

The 1257 CE eruption of Samalas also produced pyroclastic density currents (PDCs) that entered the Bali Sea in the northern and the Alas Strait in the eastern part of Lombok [11,12,24,34] and might have caused a pyroclastic density current (PDC)-triggered tsunami [35–40]. The Alas Strait separates Lombok and Sumbawa Island with an average distance of about 14 km. Its depth ranges from around 15 m in the nearshore to a maximum of 180 m in the middle of the channel. The seafloor materials in the Alas Strait are dominated by rock and sand [41]. Furthermore, the strait was connected by land until about 14 ka BP when the sea level rose up to 75 m below the present-day sea level [42–44]. Although Lombok Island is tectonically and volcanologically active, there is no evidence today of paleo-tsunamis that could have affected the surrounding islands and particularly the west coast of Sumbawa Island, whereas the 1815 CE eruption of Tambora generated a tsunami that left visible traces as far as 590 km away in Java Island [21,26]. Since the 1257 CE eruption of Samalas was of similar Volcanic Explosivity Index (VEI) as the Tambora one's, our initial hypothesis was that Samalas PDC's may have generated tsunamis that have left their traces, especially on the island of Sumbawa, since it is located only 14 km from the eastern shore of Lombok. This study's main aim is to identify in onshore sedimentary records the signature of high-energy marine floodings, then to characterize and date them to see if they can be related to the Samalas eruption of 1257 CE. This work will also be a valuable contribution to disaster risk reduction in Sumbawa and Lombok Island in the future and bring some information about tsunami recurrence rates and its origin, either from earthquakes or volcanic activities.

2. Study Area

The Lesser Sunda Islands (LSI) comprises deep oceanic trenches and several small islands, including Lombok and Sumbawa Islands (Figure 2a). The landform in Sumbawa Island is mostly mountainous areas, dating from the early Miocene until the Holocene era, with a few small low plains and small uninhabited islands in its western part (Figure 2b). Based on the last 14 years of data, normally, the study area's wave height ranges from 0.50 to 1.50 m but can exceed 2.00 m during the seasonal transition [45,46]. Currents in the study area are characterized by longshore currents with a dominant direction toward the south all year round, which its velocity can reach 1.7 m/s during the East Monsoon [34,45]. The tidal pattern in the study area is a diurnal tide, with the maximum high tide and the minimum low tide are 0.6 and −0.5 m, respectively [45]. These conditions are strengthened by other favorable hydro-oceanographic parameters, i.e., warm temperature (27–29 °C), salinity between 32–34‰, and clear waters; hence the environment is very suitable for coral reefs ecosystem. Figure 3 shows the spatial distribution of coral reefs along the Alas Strait as well as the general landscape in the form of a reef flat and reef slope on the western coast of Sumbawa [47], especially in the nearshore zone of Kiantar Village, which can play an essential role in protecting the shore and reducing the impact of marine-origins hazard events in this area, especially from wave activities.

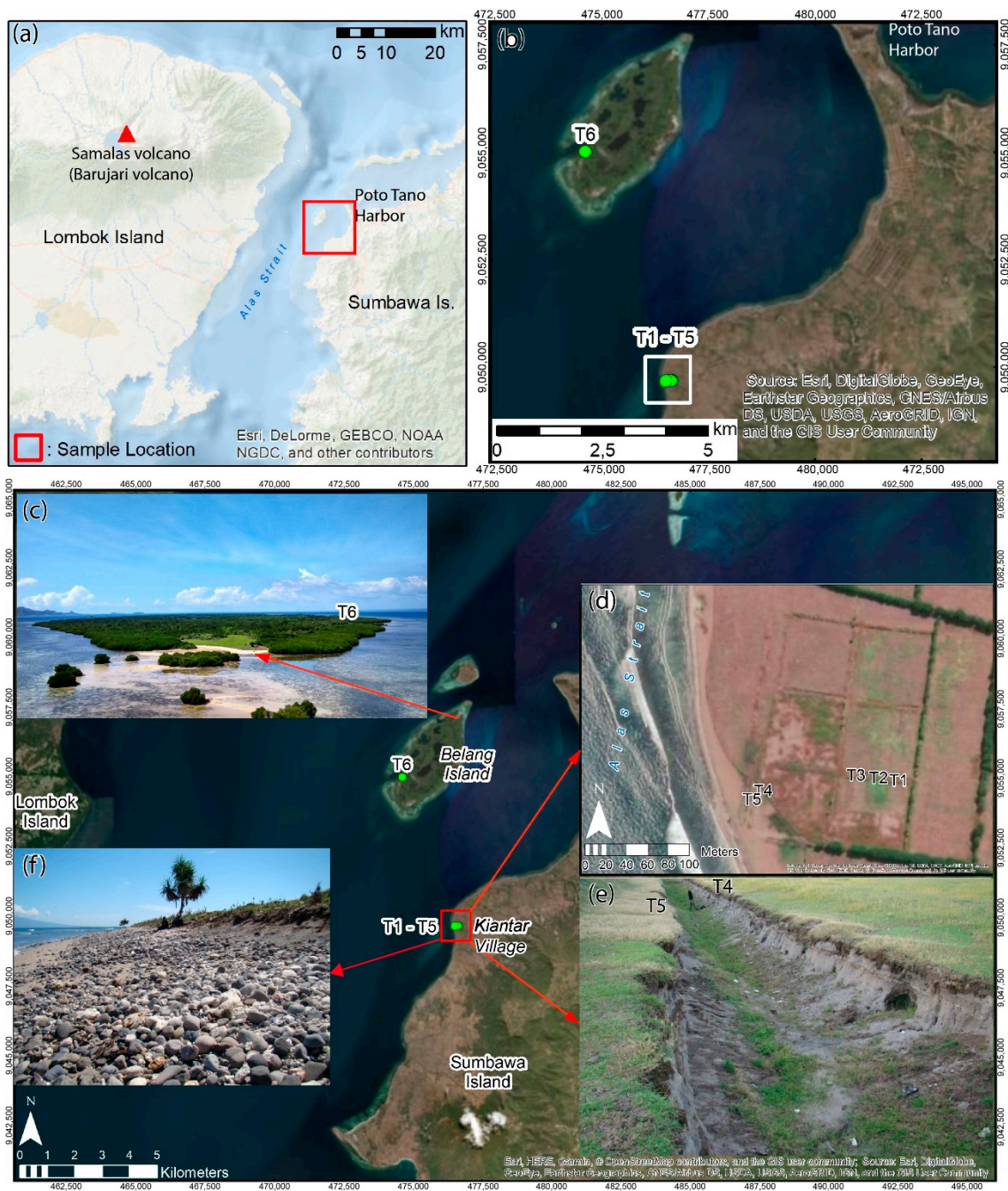


Figure 2. (a) The geographical situation of sample location in the context of Samalas volcano, Lombok, and Sumbawa Islands; (b) sample collection location in abandoned fishponds in Kiantar Village (T1–T5) and Belang Island (T6) on the western coast of West Sumbawa. Tsunami deposits in Belang Island and abandoned fishponds in Kiantar Village: (c) As a small uninhabited island located in Gili Balu conservation area on the western coast of Sumbawa, this island is dominated by mangrove ecosystems with several sandy areas; (d) sample collection location in abandoned fishponds in Kiantar Village; (e) abandoned fishponds in Kiantar Village with locations T4 and T5 sampling points as well as Alas Strait and Lombok Island to the west (left side); and (f) present-day beach materials that contain coarse rounded pebbles and coral debris.

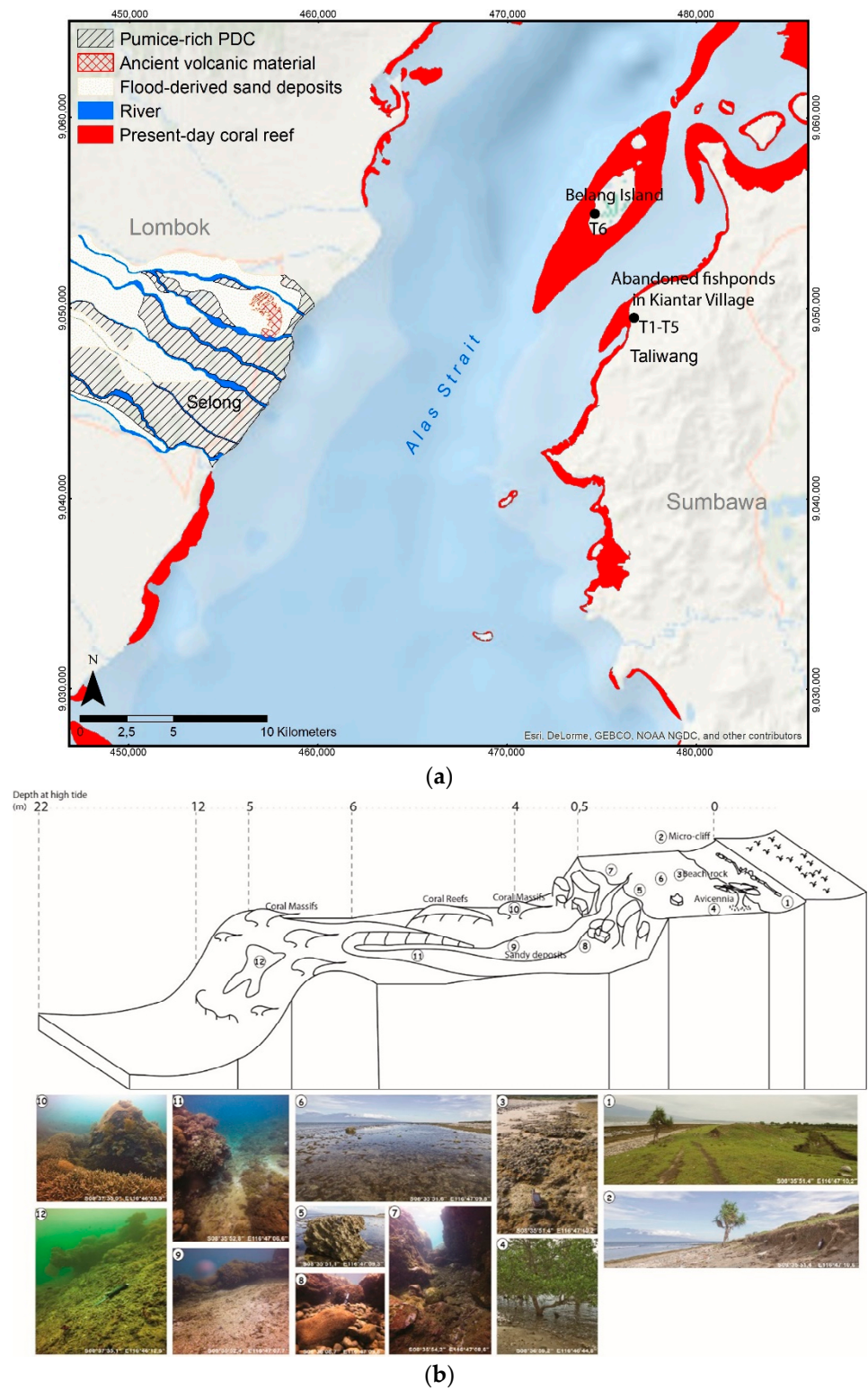


Figure 3. (a) Spatial distribution of coral reefs along the Alas Strait in the present-day (modified from [11,34]); and (b) General landscapes on the western coast of Sumbawa (courtesy of A. Landa, 2016).

Furthermore, in West Sumbawa (see Figure 1), there are 15 uninhabited islands from a total of 18 islands. We investigated Belang Island, which is one of the small uninhabited uplifted coral islands in Gili Balu district, 5 km from the main harbor of Poto Tano (Figure 2c). Stretched along a SW-NE axis on 4.5 km, the Island is characterized by flat

topography and the presence of lagoon depressions that may have acted as sediment traps where we found a marine deposit (T6), 100 m from the coastline. We also investigated south of Kiantar Village, where local residents reported the findings of numerous coral and seashell fragments while digging their wells. Sumbawa's geological map from the Indonesian Geological Agency reveals that Kiantar Village is not situated in the fault zone. The nearest fault zone is located 6 km away from the abandoned fishponds in Kiantar Village. A huge submergence coastline characterizes Saleh Bay, the largest bay in Sumbawa, 115 km away to the east from Kiantar Village. Furthermore, the nearest active volcanoes, which the expansion and changes of their magma chambers may cause uplift, even in the absence of an eruption, are situated 40 km away (Samalas volcano) and 140 km away (Tambora volcano) from Kiantar Village. Kiantar village's landform is mostly alluvium and coastal deposits from the Holocene era. In this village we found an abandoned network of large trenches recently dug to realize six 70 m × 70 m fish farming ponds located 100–300 m from the coastline. Thanks to these 1190 m of 2 m wide and 1–2 m deep trenches, we investigated thick inland marine deposits consisting of sand, pumice, pebbles, and coral rubble (T1–T5 in Figure 2d).

3. Materials and Methods

3.1. Field Surveys

Three field excursions were conducted along the littoral of West Sumbawa from 2016 to 2018 in search of anomalous beach deposits that might be a remnant of past tsunami events triggered by eruptions from the nearby volcanic system. Reports by local residents and the availability of abandoned aquaculture trenches made the sequence of deposits near Kiantar Village and in Belang Island an excellent candidate.

At selected locations (in T4—Figure 2d), eight vertically contiguous sand samples were collected from previously cleaned outcrops for further analysis, i.e., grain size analysis and analysis with the anisotropy of magnetic susceptibility (AMS) technique, which in detail will be explained in the next part. Furthermore, we collected ancient coral fragments (eight samples) and seashells (four samples) for radiocarbon dating from T1–T5 sections in abandoned fishponds in Kiantar Village and T6 section in Belang Island (see Figure 2).

3.2. Grain Size

Sediment grain-size characteristics may be used to analyze the features of tsunami deposits [48–50] since it can be used to determine trends in surface processes related to the dynamic conditions of sediment transportation and deposition. Progressing from the coast inland, we can determine, according to the characteristics of the deposits encountered, three homogeneous zones:

1. The proximal zone, closer to the sea extending substantially between the first two trenches parallel to the coast, which will be represented mainly by sections T4 and T5;
2. The intermediate zone is located between trenches 2 and 3, represented by T3, T2, and T1 sections. Given the similarity between all sections in the proximal sampling area in abandoned fishponds, Section T4 (Figure 2) was selected for grain size analysis. Grain size samples in the T4 outcrop (Figure 2e) were obtained and determined based on the sediments' visual characteristics for each homogenous layer;
3. The distal zone extends landward beyond trench 3 and can be characterized by P1 (see Figure 2d). This zone is characterized by coarse material and has very poor sandy material.

We conducted the grain-size investigation for the fine fraction of the sediments utilizing a Beckman Coulter (Indianapolis, IN, USA) LS-13-320 laser diffraction particle size analyzer device in the Laboratory of Soil Analysis, Ecole et Observatoire des Sciences de la Terre—University of Strasbourg. This laser-based technology uses the flagship multi-wavelength system, and it may analyze the sediment distributions that range from 0.017 µm to 2000 µm without the risk of sediment lost, either the largest or the smallest particles in the sediment sample. The samples pre-treatment protocol for LS13-320 is rather complex

and includes a one-week drying at 40 °C, the destruction of organic matter with hydrogen peroxide in a thermostatically controlled bath, the disaggregation, washing, and eventually the dispersion thanks to the help of sodium hexametaphosphate (detailed protocol available on request to the authors).

Grain-size analysis results encompass granulometric parameters, such as grain-size average (arithmetic mean diameter) reflecting the flow competence, sorting degree (variance and standard deviation), and form of the grain-size distribution (skewness and kurtosis), providing information on the settling processes. They are determined by the LS13-320 program from the formulas given below. Size channels in the LS13-320 are spaced logarithmically and are therefore progressively wider in span toward larger sizes. Statistical calculations are made based on the logarithmic center of each channel. Mean grain size, i.e., the surface weighted mean diameter arithmetic mean size in surface area % mode ($D_{(p,q)} = \left[\frac{\sum n_i x_i^p}{\sum n_i x_i^q} \right]^{\frac{1}{p-q}}$) reflects the ability of the flow to transport more or less large particles.

Both standard deviation which is the square root of the variance ($SD_a = \sqrt{\frac{\sum [f_i (x_i - \bar{x})^2]}{\sum f_i}}$); skewness that precise the degree of distortion from symmetry ($g_{1a} = \sqrt{\frac{\sum [f_i (x_i - \bar{x})^3]}{SD^3 \sum f_i}}$) and kurtosis, g_{2a} , which characterizes the peakedness of a distribution ($g_{2a} = \sqrt{\frac{\sum [f_i (x_i - \bar{x})^4]}{SD^4 \sum f_i}} - 3$) reflect the shape of the particle size distribution and contribute to the understanding of the sedimentation processes.

The coarse fraction of the sediments is more complex to study because it is composed of elements of two different natures: (1) Pebbles whose shape is closely linked to their mineral nature, to the processes of transport by waterways, and to their re-shaping by coastal processes. For this material, we used the “pebble count technique” developed by Wolman (1954); therefore, we sampled 30 pebbles on each site investigated (T1–T5 and P1–P3; see Figure 2d) thanks to the help of a 10 cm square mesh grid, and we measured for each element collected its intermediate axis, i.e., the axis determining the passage through a sieve mesh; and (2) Coral bioclasts whose shape is linked to their internal structure and to the fragmentation processes that have affected them during their transport ashore. For this material, there is no method established to approach their mean size statistically. To give an average idea of the competence of the waves that moved them, we have chosen to measure their largest axis, and solely the largest clasts were selected.

3.3. Dating

Twelve samples in the form of coral fragments and seashells were analyzed for radiocarbon dating at Laboratoire de Mesure du Carbone 14—LMC14 (France) and Beta Analytic and DirectAMS (United States of America). Samples of coral fragments and seashells were calibrated with Marine20 [51] and a DeltaR value of -90 ± 29 [52]. We dated eight samples of coral and four samples of seashells collected in Belang Island (BI) and abandoned fishponds during fieldworks in Kiantar Village (AF) in the time range between 2016 and 2018 with details in Table 1. In 2016, we dated two coral fragments that we sampled at both extremities of the T6 deposit in Belang Island (see Figure 2), at -35 cm (BI1) and -80 cm (BI2) from the surface, respectively.

Table 1. Samples for radiocarbon dating.

Sample Name	Sample Type	Sample Location
AF1	Seashell	T1
AF2	Seashell	T1
AF3	Seashell	T1
AF4	Coral	T3
AF5	Coral	T4
AF6	Coral	T4
AF7	Coral	T4
AF8	Coral	T3
AF9	Seashell	T2
AF10	Coral	T3
BI1	Coral	T6
BI2	Coral	T6

In 2016, we sampled seashell fragments randomly from the marine-origins deposit in Kiantar Village since we assumed that all deposits in abandoned fishponds in Kiantar Village were deposited due to the tsunami following the 1257 CE eruption of Samalas. Our assumption was based on abandoned fishponds' geographical position, which is located in front of Lombok's east coast and all the seashells fragments chronologically situated below the ashes from the 1815 CE Tambora volcano and the 1257 pumice-rich PDC from Samalas volcano. After the first sampling effort in 2016, we changed the sampling protocol in 2017 and 2018, and prefer used to dating very fresh and unbroken red coral fragments (*Tubipora musica*) to obtain better results. Nevertheless, in 2018 we still used one sample of a seashell as representative from the T2 section since we did not find any unbroken red coral fragments in the T2 section (see Figure 2). *Tubipora musica*, or the organ pipe coral, is an alcyonarian coral originally from the shallow waters and sheltered areas of the Indian Ocean. Sampling selection turned towards *Tubipora musica*, a red coral that is easier to recognize individuals with a low degree of diagenesis and a high degree of magnesium calcite, which is very suitable for dating [53].

3.4. Wave Direction

The reconstruction of the wave direction during deposition remains a key element for the accurate identification of a tsunami deposit [54]. The back and forth movement of the water is supposed to have been recorded by the sediments deposited inland during a tsunami event recording [55,56]. Determining the precise orientation of the first wave of the event makes it possible to pinpoint the event's source. The direction of subsequent waves, although roughly consistent with the first is of lesser importance because they may have been altered by reflections or refraction along the shoreline, making it more difficult to interpret. The measurement of these wave directions can be done on cobbles and pebbles by measuring their imbrication, or on much finer materials such as sand or silts using the AMS technique, which uses the magnetic properties of sediments to determine their micro-imbrication [55,57]. At the Kiantar site, the material deposited represents all the grain size classes from silts to large pebbles. Both approaches were therefore used. We carried out clast imbrication measurements (dip and orientation of the long axis of pebbles were measured on 30 randomly collected elements per site) and, when possible, took samples to assess AMS using oriented 2 cm side square plastic boxes to plug the sandy sediment and collect undisturbed material. The sampling for AMS was possible in the sandy layers between the coarse layers; hence we took eight samples for further analysis. AMS technique cannot be used on poorly cohesive and heterogeneous sediments (i.e., coarse elements included in fine sand) to reconstruct the flow direction. When the sampling box is plugged in, the sediment coarser clasts are pushed by the box walls. In this case, the resulting deformation of the original sediment fabric does not allow an accurate reconstruction of the flow direction [55].

4. Results

4.1. Belang Island

We found an intriguing deposit in the one-meter thick natural outcrop located on the western part of Belang Island (see Figure 2). In this outcrop, the first layer, located below the 15 cm-thick topsoils, is 15 cm-thick dark brown volcanic ash from the 1815 CE eruption of Tambora Volcano (−15 to −30 cm), which is ubiquitous in all the area. The layer below the volcanic ash (−30 to −90 cm), composed mainly of homogenous fine clear sand, displays an undulating contact with the volcanic ashes atop locally interrupted by 5–15 cm deep shell burrows. Below this contact, beyond a 5 cm thick ash impregnation fringe, the fine sands display on the first 15 cm with a concentration of pieces of broken coral, shells, and rounded pumices (\varnothing 3–4 cm). Between −45 and −70 cm, the sands are exempt from larger bioclasts, but below (−70 to −90 cm), appears the second layer of broken coral concentration. The top of this layer is characterized by 10 cm of coarser sands. The last layer at the bottom of the outcrop is constituted of sandy material with neither pumice nor coral fragments presence. Based on its characteristics mentioned above, we can conclude that the deposit in Belang Island is a marine origin deposit. We believe that the pumice-rich PDC was at this point too energetic to allow significant deposition on this very flat Island. Only small rounded pumices were present within the deposit. Significant deposition occurred ashore when friction increases at the base of the PDC. Figure 4 shows the stratigraphic profile of the T6 outcrop in Belang Island (see Figure 2).

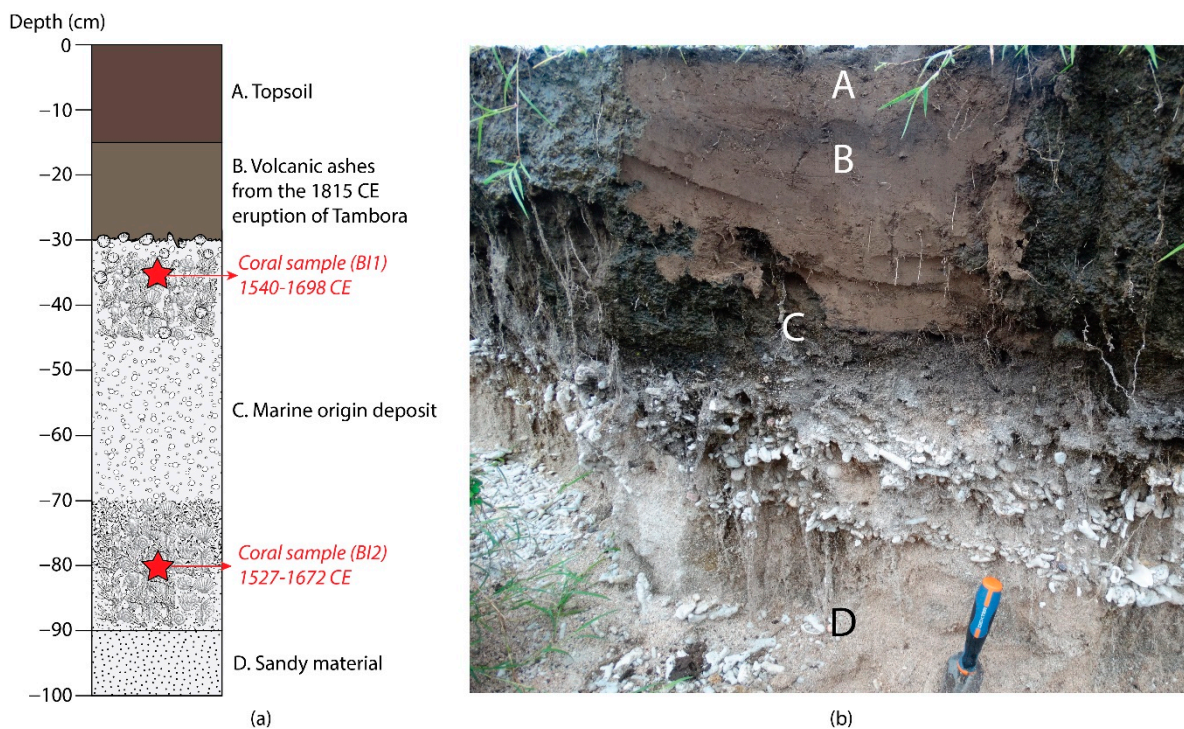


Figure 4. (a) The stratigraphic profile and (b) photo of T6 outcrop in Belang Island.

The sedimentary succession described between −30 and −90 cm from the surface is characterized by two layers of coarse sediment and large bioclasts separated by a coarse sand layer, which is not typical of a beach deposit. The presence of rounded pumice from the mid-13th century Samalas eruption proves, first, that this stratified deposit results from a marine submersion; second, that a marine submersion has emplaced it after 1257 CE. Although the hypothesis of a storm deposit cannot be totally ruled out, the strongest storms of the region do not seem able to generate marine submersion capable of transporting a large volume of sand hundreds of meters inland. Therefore, it is more likely that a tsunami

with two main waves (corresponding to the layers enriched in large bioclasts) was the cause of this 60 cm sedimentary succession.

Table 2 displays radiocarbon dating results for the coral samples in Belang Island. The results give two similar calibrated ^{14}C dates around the 16th or 17th century CE, which is consistent with a post-1257 CE event. As frequently observed, radiocarbon dates of coral fragments can provide much older dates than a tsunami event. The 60 cm-thick sedimentary deposit at Belang Island cannot be attributed to the tsunami event generated by Tambora's 1815 eruption. If this had been the case, the ashfall deposits, which were deposited before the tsunami deposit, should have been capped by marine sand or eroded by the tsunami waves. Therefore we assume that the tsunami deposit was earthquake-triggered.

Table 2. Radiocarbon dates for samples from Belang Island.

Sample Name	Sample Type	Uncal Age BP	Cal. Age CE (1 Sigma)
BI1	Coral	760 ± 30	1540–1698
BI2	Coral	790 ± 30	1527–1672

4.2. Abandoned Fishponds in Kiantar Village

Basic sedimentological characteristics for the T1–T5 outcrops (see Figures 2 and 5) in an area of $3.3 \times 10^4 \text{ m}^2$ are as follows:

1. At sampling points T1, T2, and T3 (see Figures 2 and 5a), a massive deposit of marine origin with a single ~1.5 m thick layer characterized by a dominance of large rounded blocks and pebbles roughly imbricated landward at the base with a coarse sandy matrix more or less cemented containing numerous coral and shell clasts (part A in Figures 6 and 7). This unit is topped by a mixture of abundant large smooth coral fragments and rounded pebbles in a lightly cemented sandy matrix with abundant bioclasts and whole shells (Figure 5a). The material of this upper unit displays a neat landward imbrication. This large and massive deposit ends on a very short distance, i.e., between 200 and 250 from the sea. Investigations conducted further landward did not allow to find more than that distance; a weak layer of fine sands mixed with silts containing small shell debris detectable along the road, South of Kiantar, 300 m beyond the limit of the coarse deposit;
2. At sampling points of T4 and T5 (see Figures 2 and 5b), additional thick deposits of marine origin are composed of three different layers without paleo-sols between each layer (part B,C,D in Figure 6). Each of these layers, 0.5 m thick on average, consists of coral fragments and marine shells mixed with boulders and capped by sand (Figure 5b);
3. The uppermost geologic unit for all sampling points consists of 2 cm-thick small rounded pumice, originating from the 1257 CE eruption of Samalas (part E in Figure 6) and 20 cm tephra fall originated from the 1815 CE eruption of Tambora (part F in Figure 6) covered by topsoil (part G in Figure 6).

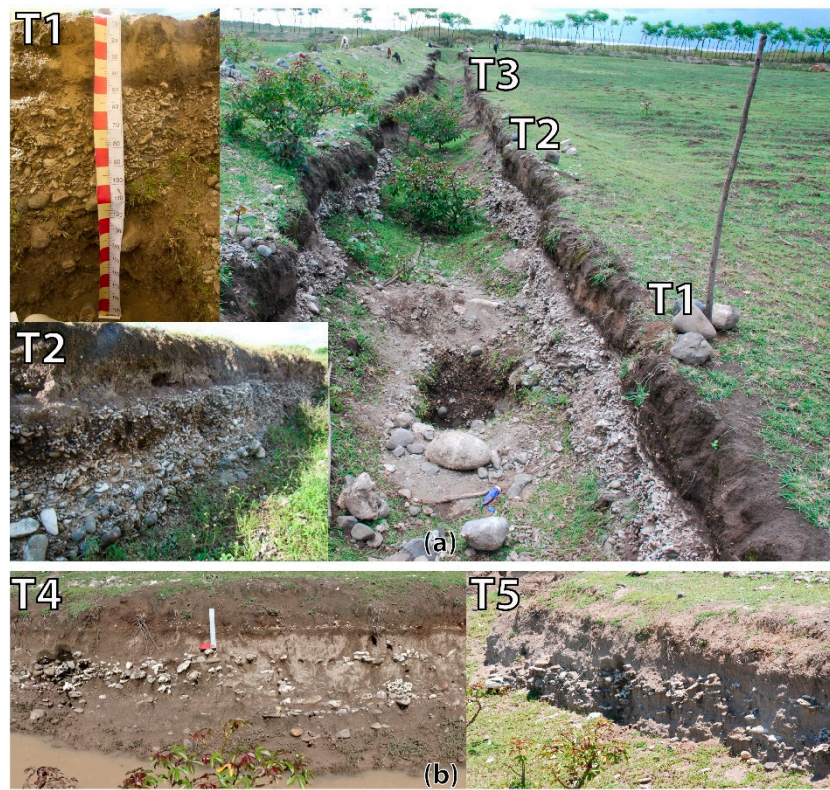


Figure 5. (a) The locations of T1, T2, and T3 sampling points (oriented seaward from T1 to T3) in an abandoned fishpond in Kiantar Village with an example of a massive tsunami deposit with a single ~1.5 m thick layer on the sampling point of T1 and T2; (b) The locations of T4 and T5 sampling points with three different layers of marine-origins deposits without paleo-sols between each layer.

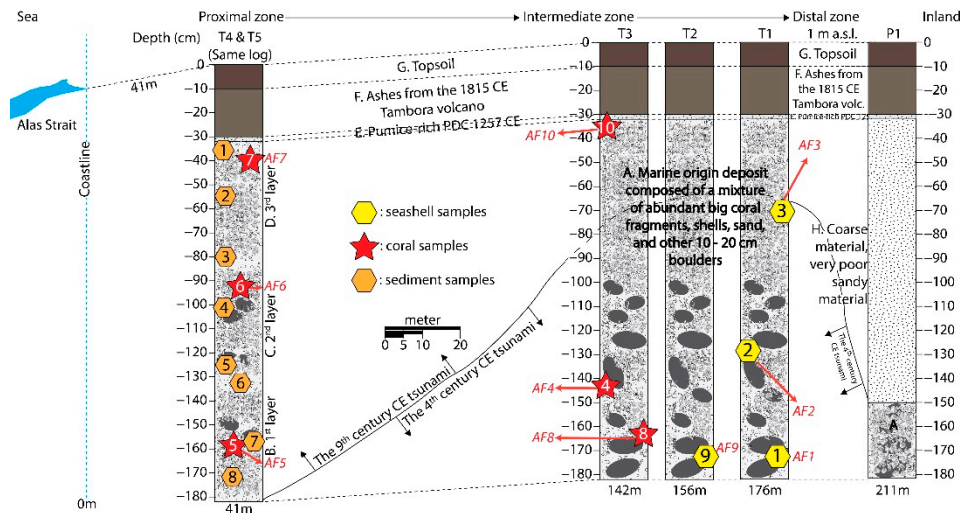


Figure 6. Stratigraphic profiles for all sampling points in abandoned fishponds in Kiantar Village.

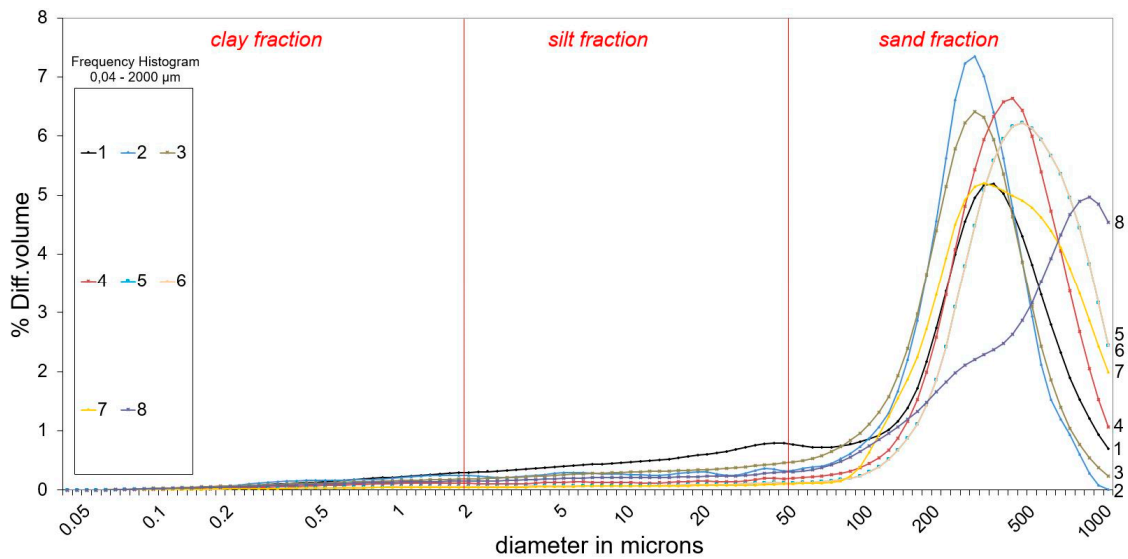


Figure 7. Textural type percentages from T4 outcrop (see Figure 6).

Figure 6 illustrates the stratigraphic profiles for all sampling points in the abandoned fishponds in Kiantar Village. The grain size results presented in Table 3 and Figure 7 show that deposits consist of medium to fine sand. The standard deviation of eight layers of sediment ranges from $\sigma\Phi$ 0.91 to 2.40, which are classified as interval $\sigma\Phi$ 0.71–4.00 [58], indicating the moderately sorted to very poorly sorted sediment layers [58,59], as usually discovered in debris flows and tsunami deposits [60,61]. Skewness ranging from S_{KI} -0.60 to -0.06 means that the sediment layers are generally composed of strongly coarse skewed to near symmetrical particles [58,59]. Furthermore, the range of kurtosis (KG 1.02–3.02) displays the curves between mesokurtic (KG 0.90–1.11) and extremely leptokurtic (KG > 3.00) [58,59]. Grain-size characteristics of tsunami deposits are commonly fining upwards within the deposits the last waves being less energetic [50,62,63] and the material is poorly sorted [48,64,65].

Table 3. Statistical parameters and textural type percentages from the T4 outcrop (see Figure 6).

Sample Name	Depth (cm)	Mean Grain-Size		Standard Deviation ($\sigma\Phi$)	Skewness (S_{KI})	Kurtosis (KG)	Textural Types Percentage (%)		
		Φ	μm				Clay	Silt	Sand
1	–35	2.95	234.83	2.40	–0.60	1.36	4.49	17.71	77.80
2	–55	2.45	225.60	1.81	–0.59	3.02	4.60	9.50	85.90
3	–80	2.50	223.54	1.76	–0.57	2.25	3.62	10.65	85.73
4	–102	1.70	347.67	1.29	–0.40	1.91	2.23	4.71	93.06
5	–125	1.70	342.80	0.91	–0.10	1.28	0.93	2.75	96.32
6	–133	1.33	446.53	0.95	–0.18	1.14	1.07	2.78	96.16
7	–157	1.56	389.93	0.98	–0.06	1.02	0.95	2.32	96.73
8	–172	1.38	548.53	2.01	–0.48	1.61	2.95	7.41	89.64

For coarse material, the pebble count data (Table 4) show that the pebbles’ mean size increases landward to reach a maximum in the last trench inland in P1 (see Figures 2d and 6), which also corresponds to the front of the thick coarse deposit. Imbrication measurements were performed on coarse material at different sections within the body of the thick deposit that can be seen beyond the second trench landward. These imbrication data represented in rose diagrams evidence a neat eastbound flow with quite no lateral dispersion (Figure 8). On the T4 outcrop, the AMS sampling was possible in the sandy layers between the coarse layers. The 8 samples of AMS from the T4 outcrop show that the sandy material was deposited in low energetic conditions. The main axis (K1) of the anisotropy ellipsoid does not displays a significant tilting and remains quite horizontal for all the samples, which means

that the flow velocity was very weak and that settling processes were dominating during sediment deposition. These conditions cannot allow reconstructing the flow direction as it can be possible with a neat tilting of this K1 axis but only show the orientation of the displacement axis, which was E–W, i.e., conform of the water movement landward that led to the large clasts imbrication. Table 3 shows that the grain size of the sand deposited at site T4 regularly decreases from the base to the top. Additionally, AMS data confirm that the fine sandy sediments were emplaced during a calm episode that favors settling in a non-turbulent context (Figure 9).

Table 4. Evolution of the sizes of the diameter of pebbles from the sea to the interior in Kiantar Village (see Figure 2d).

	T4	T3	P3	T2	P2	T1	P1
Mean intermediate axis (cm) for 30 samples	10.5	11.2	11.1	10.1	13.2	13.9	15.2

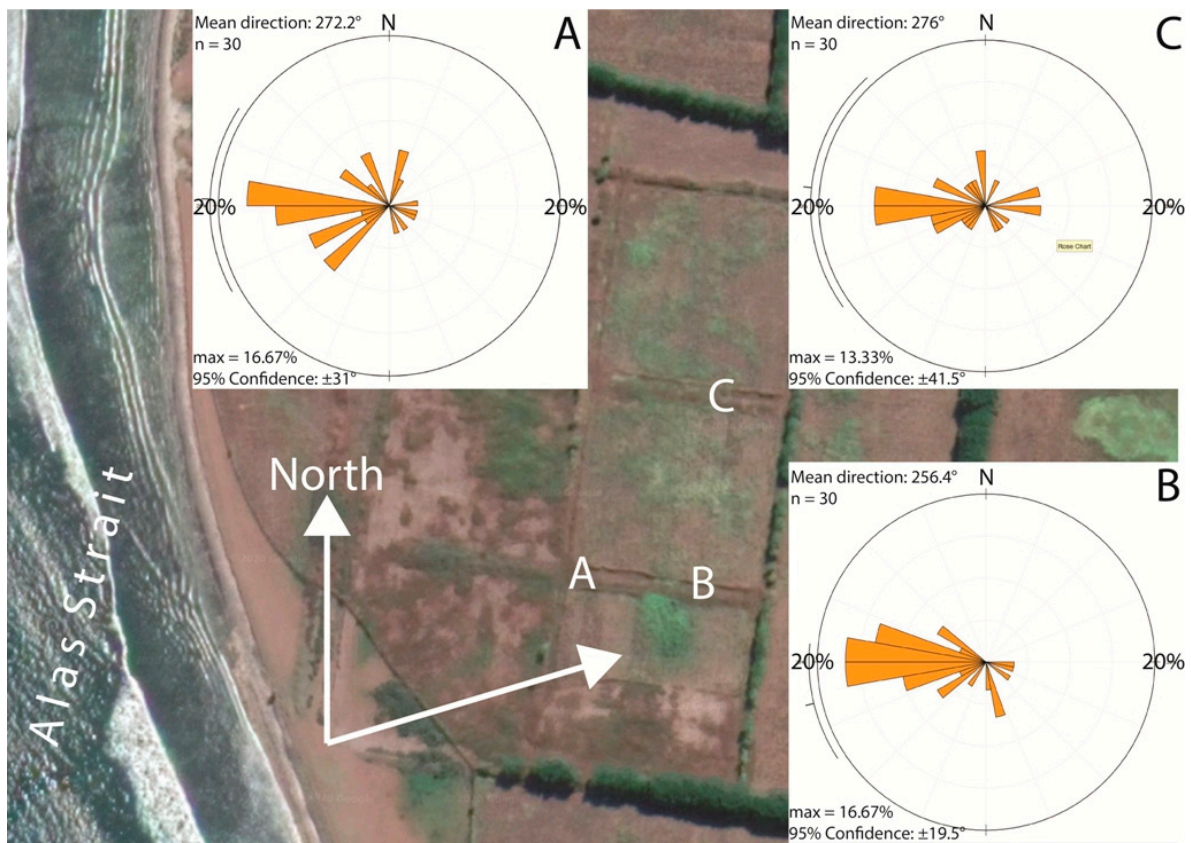


Figure 8. Imbrication measurements evidence for coarse material in abandoned fishponds in Kiantar Village.

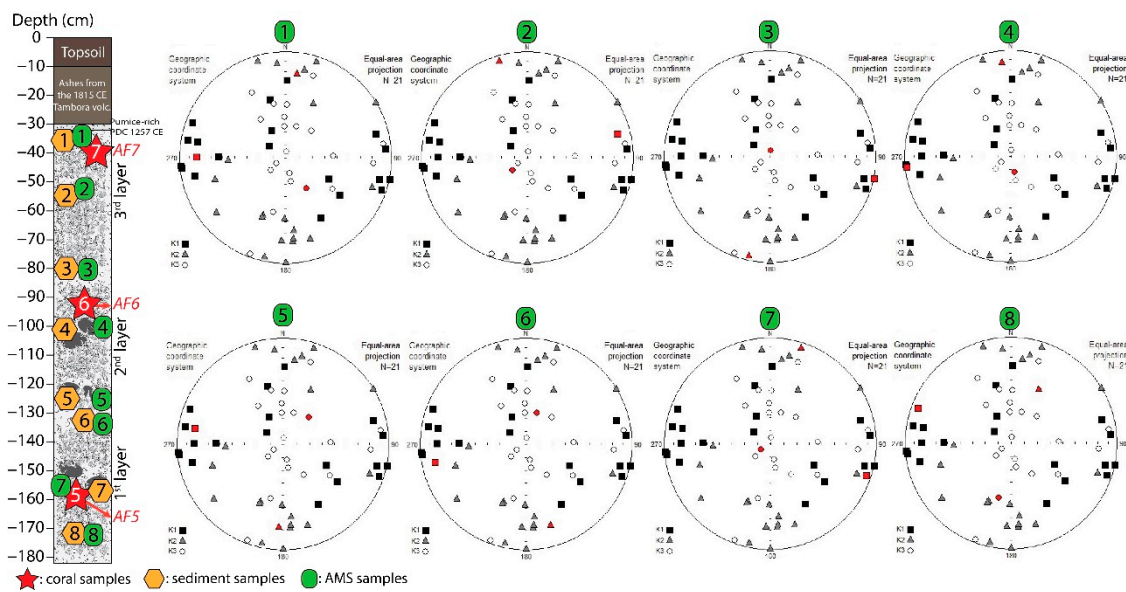


Figure 9. AMS data from T4 which confirm that the fine sandy sediments were emplaced during a calm episode that favors settling in a non-turbulent context in abandoned fishponds in Kiantar Village.

Table 5 show radiocarbon dating results for the coral and seashell samples in Kiantar Village. Following the 2016 fieldworks, we focused more on coral fragments as radiocarbon dating results for the 2016 samples had no significant results since the year obtained are too distant from our hypothesis, i.e., 1257 CE. Based on the radiocarbon dating results in Table 5, it shows that we have two clusters of dates that stand out: ~1500 BP and 2000–2300 BP.

Table 5. Radiocarbon dates for samples from the abandoned fishponds in Kiantar Village.

Sample	Date of Analysis	Sample Type	Outcrop	Depth (cm)	Uncal Age BP	Cal. Age BCE/CE (1 Sigma)
AF1	08/2016	Seashell	T1	−173	2375 ± 30	75 BCE–103 CE
AF2	08/2016	Seashell	T1	−128	2145 ± 30	216–381 CE
AF3	08/2016	Seashell	T1	−70	2250 ± 30	83–248 CE
AF4	10/2017	Coral	T3	−143	2050 ± 30	316–489 CE
AF5	10/2017	Coral	T4	−158	1520 ± 30	879–1031 CE
AF6	10/2017	Coral	T4	−92	1540 ± 30	854–1010 CE
AF7	10/2017	Coral	T4	−40	1560 ± 30	883–992 CE
AF8	12/2017	Coral	T3	−162	2169 ± 40	174–355 CE
AF9	12/2017	Seashell	T2	−172	2137 ± 34	225–392 CE
AF10	03/2018	Coral	T3	−35	1740 ± 28	654–789 CE

5. Discussion

Based on stratigraphic profiles for all sampling points in the abandoned fishponds in Kiantar Village (T1–T5; see Figures 2 and 6), there is a clear sequence represented by ten centimeters of topsoil overlying ~20 cm thick ash that correlates to the widely identified to the 1815 CE Tambora volcano eruption [31,32]. Beneath this layer, there is a thick (minimum 140 cm) deposit of mixed shell, sand, and cobbles resembling materials commonly seen in the shallows and beach areas immediately offshore. The large deposit found in T1–T3 (a single massive ~1.5 m thick layer; see Figures 5a and 6) seems to corresponds to the dam of a reverse debris flow (moving landward) generated by very strong turbulent flow coming from the sea. This debris flow-like deposit comprises unsorted coarse material collected on the seashore (attested by the same material visible on the current beach: coarse rounded pebbles and coral debris) and deposited in mass (with a landward imbrication of the material as can be seen in Figure 5a, T2). Additionally, the pebbles’ mean size increases landward, and the largest stones can be found on the front mass of debris at the level of

the last trench inland (P1; see Figures 2d and 6, and Table 4), where the thickness of the deposit drops abruptly to 0.3–0.4 m. The increase in the size of the elements constituting the deposit with the distance to the sea would be inverse to the logic if the material had been transported in a Newtonian flow but becomes consistent with a Bingham-type behavior where the large elements are bulldozed on the front of the flow. This similarity between the behavior of tsunamis inland and that of debris flows in the mountains is common, and it is certainly not without reason that the Japanese often use the term Yama tsunami to refer to debris flows in the mountains or on the sides of volcanoes.

As an extension of this deposit, 550 m from the coastline, a description of a 1 m deep trench along the road embankment south of Kiantar Village shows a total absence of large clasts and a dominance of fine sands, which confirms the debris flow behavior over a short distance [66]. Both grain size data, AMS, and the evidence of coarse material transported in mass over a short distance confirm that high energy marine floodings occurred on the flat plain of the Kiantar area in the past.

Dating results for coral and seashell samples in the abandoned fishponds emphasize that at least two different tsunamis occurred along the western coast of Sumbawa (Figure 10), i.e.,:

1. Tsunami deposits probably dated 4th century CE (the most recent date), based on six samples, namely AF1, AF2, AF3, AF4, AF8, and AF9. We concluded that all coral and seashell samples from sampling points T1, T2, and T3 (see Figures 5 and 6) were deposited following the same event since their deposits have the same visual characteristics, i.e., a single massive ~1.5 m thick layer displaying clear clast imbrication landward, large dense blocks, and pebbles at the base and less dense broken coral atop with locally a flatter fabric. Debris flows often develop reverse grading due an intense shearing at the base during transport, leading to the formation of dispersive pressure of shearing oriented upward. It is not the case here while the short distance between the source of the sediments and their deposition did not allow the reverse grading to occur. Furthermore, the deposits are too thick to have been deposited by a single storm and, also, large storms are infrequent in the study area since it is situated in a protected narrow strait with low wave ranges [45,46];
2. The 9th century CE tsunami, based on coral samples at sampling point T4 (AF5, AF6, and AF7; see Figures 5 and 6) and AF10, since dating results using the most suitable sampling protocol showed the same range years for each layer. This tsunami deposit overlay the deposit of the 4th-century tsunami and outcrops in all the proximal zone, i.e., between the first and the second trench. Its internal structure corresponds to three pulses' records characterized each by a phase of strong energy when the turbulent wavefront favors transport and deposition of coarse pebbles. A laminar flow follows this phase during the wave tail passage that allows fine sediments to settle.

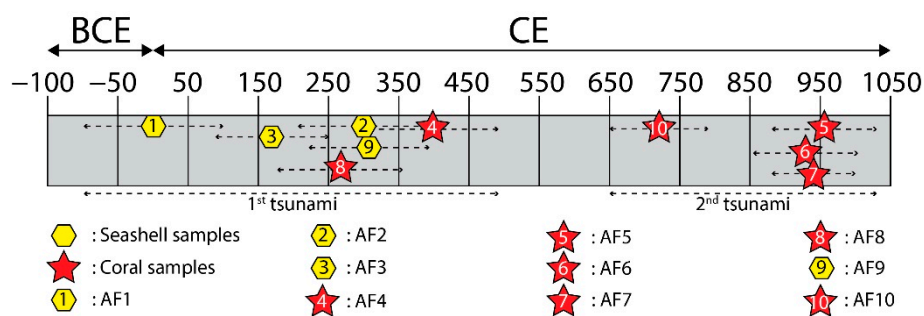


Figure 10. Dating results for coral and seashell samples in the abandoned fishponds in Kiantar Village.

Radiocarbon dating results have shown that volcanic materials from the 1257 CE eruption of Samalas volcano that reached the sea did not trigger a massive tsunami on the western coast of Sumbawa. Although the volume of pumice-rich PDCs on the eastern part of Lombok in the aftermath of the 1257 CE eruption was found to be approximately

$4435 \times 10^6 \pm 5.5 \text{ m}^3$ [11], volcanic materials that reached the sea did not induce a significant tsunami since no deposits were found on the western coast of Sumbawa. The layer of pumice materials found in the T1–T5 (Figure 7) is originated from the fallout processes, not from the tsunami [11,24,31,32].

The sandy layer on Belang Island has been deposited by a flow direction of which is roughly in accordance with the direction of the waves generated by the entrance of the 1257 CE pyroclastic flows into the Alas Strait. The 17° tilting of the main axis of the AMS ellipsoid (K1) is consistent with the transport of the material in a hyper concentrated flow at the base of the water column and compatible with a low energy tsunami. Nevertheless, the unique signature of this weak tsunami did not correspond with dating results, i.e., 1540–1698 CE and 1527–1672 CE. Therefore, deposits in Belang Island are not the results from a tsunami triggered by the 1257 CE eruption of Samalas, as already mentioned.

Since it was an insignificant tsunami, then it is reasonable that no deposits were found on the western coast of Sumbawa. At least three factors may explain the limited wave height and run-up of this tsunami: (1) the tsunami source velocity: the 1257 CE PDCs already had a limited velocity when reaching the Alas Strait, about 30 km away from the Samalas crater; (2) the nature of the PDC deposits: the very light pumice fragments of the PDCs certainly did not provide sufficient strength to push the seawater efficiently and will float in the water; (3) coral barrier: coral reefs along the Alas Strait served as an effective barrier against tsunamis and may have reduced their impacts on the coastal area [67–70].

There is presently no living coral near the coast on the eastern part of Lombok, especially in front of Selong, where great amounts of pumice-rich PDCs from the 1257 CE eruption entered the Alas Strait [34] (see Figure 3a). Although the present-day conditions of the reefs on the eastern part of Lombok and the western part of Sumbawa are very different, we assumed that, before the eruption of Samalas volcano in 1257 CE, coral reefs in this area were in good condition. This condition may have resulted in the absence or limited presence of tsunami deposits from the 1257 CE eruption in this area. Additionally, we conclude that pre-1257 CE coral reefs, especially near Selong, were buried by volcanic materials following the 1257 CE eruption since there were dead corals and white sand below the 1257 CE pumice layer at several wells near the coast [11]. Furthermore, the regular input of acid pumice material transported in suspension by the main rivers in this area has affected the coral presence since then [34]. On the contrary, present-day coral reefs on the western coast of Sumbawa are in good condition. We assume that the pre-1257 CE coral reef in this area was also in good condition since, as mentioned in the local written sources called Babad Suwung, there was no human civilization until someone from Lombok Island named Amaq Talkuwang arrived in this area [24]. Therefore, anthropogenic pressures that cause coral bleaching or direct destruction did not exist in this area. Coral reefs as barriers within two meters of the water surface and located at least a few hundred meters separated from the main island can perform a significant role in reducing tsunami effects [34,69,71,72], including in the case of following the 1257 CE Samalas eruption.

6. Conclusions

Deposits found on the western coast of Sumbawa have common characteristics with tsunami deposits, such as fining upwards within the deposits as well as poor sorting of sediments. Here, due to the huge amount of coarse sediments collected on the seashore, the material was transported in mass over a short distance and deposited in mass explaining the poor sorting that characterized this deposit. A single weak layer of fine sands was found inland, 500 m beyond the limit of coarse material deposit

For the last millennium, three tsunamis have struck the western coast of Sumbawa, dated 4th century CE, 9th century CE, and 17th century CE, some of the deposits of which were found in abandoned fishponds in Kiantar Village and Belang Island. We conclude that these tsunamis were earthquake-triggered tsunamis, since there were no volcanic eruptions occurring in the area at that time [73,74]. Although the 1257 CE eruption of the Samalas volcano generated more than 4 km^3 of volcanic materials, the 1257 CE material could only

trigger an insignificant tsunami along the western coast of Sumbawa Island. Several factors may result in this insignificant tsunami, i.e., bathymetry, tsunami source velocity, type of tsunami source material, and a coral reef presence in that area.

Further in-depth studies related to paleo earthquake-triggered tsunamis are needed since (1) there have been no studies as yet about these events; (2) it is essential in the current seismic context, where people fear tsunamis, and, (3) it also can provide detailed information on paleo tsunami events along the western coast of Sumbawa. This information will be handy for disaster risk reduction in Sumbawa as well as Lombok Island in the future.

Author Contributions: Conceptualization: B.W.M., F.L., and P.W.; data curation: B.W.M., F.L., P.W., M.T., C.G., and B.S.; formal analysis: B.W.M., F.L., P.W., C.G., and D.S.H.; funding acquisition: F.L.; investigation: B.W.M., F.L., P.W., M.T., P.J., B.S., J.-C.K., and J.S.; methodology: B.W.M., F.L., P.W., M.T., B.S., J.-C.K., and J.S.; project administration: F.L. and D.S.H.; software: C.G.; supervision: F.L.; visualization: B.W.M. and C.G.; writing—original draft: B.W.M., F.L., P.W., M.T., P.J., C.G., B.S., J.-C.K., J.S., and D.S.H.; writing—review and editing: B.W.M., F.L., P.W., M.T., P.J., C.G., B.S., J.-C.K., J.S., and D.S.H. All authors have read and agreed to the published version of the manuscript.

Funding: Fieldwork and data analysis were co-funded by Université Paris 1 Panthéon Sorbonne (AAP Politique Scientifique), the Centre National de la Recherche Scientifique (CNRS–PICS n°260868), and the Australian Research Council (Linkage Project LP150100649) led by Murdoch University.

Institutional Review Board Statement: Not applicable.

Informed Consent Statement: Not applicable.

Data Availability Statement: Data is contained within the article.

Acknowledgments: This paper has been written as part of a collaborative project between Universitas Gadjah Mada and Université Paris 1 Panthéon Sorbonne. We wish to thank Adrien Landa, Lalu Syafi'i, and Lalu Sugi for participating in the fieldwork. The authors dedicate this article to Sunarto, Hartono, and Didi Kempot, who passed away recently. Finally, the authors would also like to thank anonymous reviewers for their helpful comments on this paper.

Conflicts of Interest: The authors declare no conflict of interest.

References

1. Tsushima, H.; Hirata, K.; Hayashi, Y.; Tanioka, Y.; Kimura, K.; Sakai, S.; Shinohara, M.; Kanazawa, T.; Hino, R.; Maeda, K. Near-field tsunami forecasting using offshore tsunami data from the 2011 off the Pacific coast of Tohoku Earthquake. *Earth Planets Space* **2011**, *63*, 56. [\[CrossRef\]](#)
2. Gusiakov, V.K. Relationship of Tsunami Intensity to Source Earthquake Magnitude as Retrieved from Historical Data. *Pure Appl. Geophys.* **2011**, *168*, 2033–2041. [\[CrossRef\]](#)
3. Lobkovsky, L.I.; Baranov, B.V.; Dozorova, K.A.; Mazoza, R.K.; Kisel'man, B.A.; Baranova, N.A. The Komandor seismic gap: Earthquake prediction and tsunami computation. *Oceanology* **2014**, *54*, 519–531. [\[CrossRef\]](#)
4. Satake, K. Advances in earthquake and tsunami sciences and disaster risk reduction since the 2004 Indian Ocean tsunami. *Geosci. Lett.* **2014**, *1*, 15. [\[CrossRef\]](#)
5. Thurman, H.V.; Trujillo, A.P. *Essentials of Oceanography*, 11st ed.; Prentice Hall: Upper Saddle River, NJ, USA, 1999; p. 527.
6. Begét, J.E. Volcanic tsunamis. In *Encyclopedia of Volcanoes*; Sigurdsson, H., Houghton, B., McNutt, S.R., Rymer, H., Stix, J., Eds.; Academic Press: New York, NY, USA, 2000; pp. 1005–1013.
7. Bryan, S.E.; Cook, A.; Evans, J.P.; Colls, P.W.; Wells, M.G.; Lawrence, M.G.; Jell, J.S.; Greig, A.; Leslie, R. Pumice rafting and faunal dispersion during 2001–2002 in the Southwest Pacific: Record of a dacitic submarine explosive eruption from Tonga. *Earth Planet. Sci. Lett.* **2004**, *227*, 135–154. [\[CrossRef\]](#)
8. Gillespie, R.; Clague, D. *Encyclopedia of Islands*; University of California Press: Berkeley, CA, USA, 2009; p. 1111.
9. Paris, R.; Wassmer, P.; Lavigne, F.; Belousov, A.; Belousova, M.; Iskandarsyah, Y.; Benbakkar, M.; Ontowirjo, B.; Mazzoni, N. Coupling eruption and tsunami records: The Krakatau 1883 case-study, Indonesia. *Bull. Volcanol.* **2014**, *76*, 814. [\[CrossRef\]](#)
10. Smart, G.M.; Crowley, K.H.M.; Lane, E.M. Estimating tsunami run-up. *Nat Hazards* **2016**, *80*, 1933–1947. [\[CrossRef\]](#)
11. Mutaqin, B.W.; Lavigne, F.; Sudrajat, Y.; Handayani, L.; Lahitte, P.; Vermoux, C.; Hadmoko, D.S.; Komorowski, J.-C.; Hananto, N.D.; Wassmer, P. Landscape Evolution on the Eastern Part of Lombok (Indonesia) related to the 1257 CE Eruption of the Samalas Volcano. *Geomorphology* **2019**, *327*, 338–350. [\[CrossRef\]](#)
12. Mutaqin, B.W.; Lavigne, F.; Hadmoko, D.S.; Malawani, M.N. Volcanic Eruption-Induced Tsunami in Indonesia: A Review. *IOP Conf. Ser. Earth Environ. Sci.* **2019**, *256*, 012023. [\[CrossRef\]](#)

13. NOAA National Centers for Environmental Information. National Geophysical Data Center/World Data Service: NCEI/WDS. Global Historical Tsunami Database. 2020. Available online: <https://data.unep-wcmc.org/datasets/1> (accessed on 20 May 2020). [[CrossRef](#)]
14. Simons, W.; Socquet, A.; Vigny, C.; Ambrosius, B.; Haji Abu, S.; Promthong, C.; Subarya, C.; Sarsito, D.A.; Matheussen, S.; Morgan, P.; et al. A decade of GPS in Southeast Asia: Resolving Sundaland motion and boundaries. *J. Geophys. Res. Solid Earth* **2007**, *112*, B06420. [[CrossRef](#)]
15. Ferrario, M.F. Landslides triggered by multiple earthquakes: Insights from the 2018 Lombok (Indonesia) events. *Nat. Hazards* **2019**, *98*, 575–592. [[CrossRef](#)]
16. Ramdani, F.; Setiani, P.; Setiawati, D.A. Analysis of sequence earthquake of Lombok Island, Indonesia. *Prog. Disaster Sci.* **2019**, *4*, 100046. [[CrossRef](#)]
17. Song, R.; Hattori, K.; Zhang, X.; Sanaka, S. Seismic-ionospheric effects prior to four earthquakes in Indonesia detected by the China seismo-electromagnetic satellite. *J. Atmos. Sol. Terr. Phys.* **2020**, *205*, 105291. [[CrossRef](#)]
18. Yang, X.; Singh, S.C.; Tripathi, A. Did the Flores backarc thrust rupture offshore during the 2018 Lombok earthquake sequence in Indonesia? *Geophys. J. Int.* **2020**, *221*, 758–768. [[CrossRef](#)]
19. Rampino, M.R.; Self, S. Historic eruptions of Tambora (1815), Krakatau (1883), and Agung (1963), their stratospheric aerosols, and climatic impact. *Quat. Res.* **1982**, *18*, 127–143. [[CrossRef](#)]
20. Stothers, R.B. Density of fallen ash after the eruption of Tambora in 1815. *J. Volcanol. Geotherm. Res.* **2004**, *134*, 343–345. [[CrossRef](#)]
21. Kandlbauer, J.; Sparks, R.S.J. New estimates of the 1815 Tambora eruption volume. *J. Volcanol. Geotherm. Res.* **2014**, *286*, 93–100. [[CrossRef](#)]
22. Sigl, M.; Winstrup, M.; McConnell, J.R.; Welten, K.C.; Plunkett, G.; Ludlow, F.; Büntgen, U.; Caffee, M.; Chellman, N.; Dahl-Jensen, D.; et al. Timing and climate forcing of volcanic eruptions for the past 2500 years. *Nature* **2015**, *523*, 543–549. [[CrossRef](#)]
23. Rössler, O.; Brönnimann, S. The effect of the Tambora eruption on Swiss flood generation in 1816/1817. *Sci. Total Environ.* **2018**, *627*, 1218–1227. [[CrossRef](#)]
24. Mutaqin, B.W.; Lavigne, F. Oldest Description of a Caldera-forming Eruption in Southeast Asia Unveiled in Forgotten Written Sources. *GeoJournal* **2019**, in press. [[CrossRef](#)]
25. Latter, J.H. Tsunamis of volcanic origin: Summary of causes, with particular reference to Krakatoa, 1883. *Bull. Volcanol.* **1981**, *44*, 467–490. [[CrossRef](#)]
26. Stothers, R.B. The Great Tambora Eruption in 1815 and Its Aftermath. *Science* **1984**, *224*, 1191–1198. [[CrossRef](#)] [[PubMed](#)]
27. Sigurdsson, H.; Carey, S. Plinian and co-ignimbrite tephra fall from the 1815 eruption of Tambora volcano. *Bull. Volcanol.* **1989**, *51*, 243–270. [[CrossRef](#)]
28. Oppenheimer, C. Climatic, environmental and human consequences of the largest known historic eruption: Tambora volcano (Indonesia) 1815. *Prog. Phys. Geogr.* **2003**, *27*, 230–259. [[CrossRef](#)]
29. Liang, E.; Dawadi, B.; Pederson, N.; Piao, S.; Zhu, H.; Sigdel, S.R.; Chen, D. Strong link between large tropical volcanic eruptions and severe droughts prior to monsoon in the central Himalayas revealed by tree-ring records. *Sci. Bull.* **2019**, *64*, 1018–1023. [[CrossRef](#)]
30. Kim, S.-J.; Kim, B.-M. Ocean Response to the Pinatubo and 1259 Volcanic Eruptions. *Ocean Polar Res.* **2012**, *34*, 305–323. [[CrossRef](#)]
31. Lavigne, F.; Degeai, J.-P.; Komorowski, J.-C.; Guillet, S.; Robert, V.; Lahitte, P.; Oppenheimer, C.; Stoffel, M.; Vidal, C.M.; Suroño; et al. Source of the great A.D. 1257 mystery eruption unveiled, Samalas volcano, Rinjani Volcanic Complex, Indonesia. *Proc. Natl. Acad. Sci. USA* **2013**, *110*, 16742–16747. [[CrossRef](#)]
32. Vidal, C.M.; Komorowski, J.-C.; Métrich, N.; Pratomo, I.; Kartadinata, N.; Prambada, O.; Michel, A.; Carazzo, G.; Lavigne, F.; Rodysill, J.; et al. Dynamics of the major Plinian eruption of Samalas in 1257 A.D. (Lombok, Indonesia). *Bull. Volcanol.* **2015**, *77*, 73. [[CrossRef](#)]
33. Guillet, S.; Corona, C.; Stoffel, M.; Khodri, M.; Lavigne, F.; Ortega, P.; Eckert, N.; Sielenou, P.D.; Daux, V.; Churakova (Sidorova), O.V.; et al. Climate response to the Samalas volcanic eruption in 1257 revealed by proxy records. *Nat. Geosci.* **2017**, *10*, 123–128. [[CrossRef](#)]
34. Mutaqin, B.W. Spatial Analysis and Geomorphic Characteristics of Coral Reefs on the Eastern Part of Lombok, Indonesia. *Geogr. Tech.* **2020**, *15*, 202–211. [[CrossRef](#)]
35. Choi, B.H.; Pelinovsky, E.; Kim, K.O.; Lee, J.S. Simulation of the trans-oceanic tsunami propagation due to the 1883 Krakatoa volcanic eruption. In *Tsunamis*, Tinti, S., Pelinovsky, E. *Nat. Hazards Earth Syst. Sci.* **2003**, *3*, 321–332. [[CrossRef](#)]
36. Freundt, A. Entrance of Hot Pyroclastic Flows into the Sea: Experimental Observations. *Bull. Volcanol.* **2003**, *65*, 144–164. [[CrossRef](#)]
37. Lander, J.F.; Whiteside, L.S.; Lockridge, P.A. Two Decades of Global Tsunamis, 1982–2002. *Sci. Tsunami Hazards* **2003**, *21*, 3–88.
38. Pelinovsky, E.; Zahibo, N.; Dunkley, P.; Edmonds, M.; Herd, R.; Talipova, T.; Kozelkov, A.; Nikokina, I. Tsunami Generated by the Volcano Eruption on July 12–13, 2003 at Montserrat, Lesser Antilles. *Sci. Tsunami Hazards* **2004**, *22*, 44–57.
39. Pararas-Carayannis, G. Risk assessment of tsunami generation from active volcanic sources in the eastern Caribbean region. In *Caribbean Tsunami Hazard, Proceedings of the NSF Caribbean Tsunami Workshop, Singapore, 30–31 March 2004*; Mercado-Irizarry, A., Liu, P., Eds.; World Scientific Publishing Co.: Singapore, 2006; pp. 91–137. [[CrossRef](#)]

40. Mattioli, G.S.; Voight, B.; Linde, A.T.; Sacks, I.S.; Watts, P.; Widiwijayanti, C.; Young, S.R.; Hidayat, D.; Elsworth, D.; Malin, P.E.; et al. Unique and remarkable dilatometer measurements of pyroclastic flow-generated tsunamis. *Geology* **2007**, *35*, 25–28. [[CrossRef](#)]
41. Schmitz, W.J. *On the World Ocean Circulation: Volume II*; Technical Report WHOI-96-08; Woods Hole Oceanographic Institution: Woods Hole, MA, USA, 1996.
42. Voris, H.K. Maps of Pleistocene Sea Levels in South East Asia: Shorelines, River Systems, Time Durations. *J. Biogeogr.* **2000**, *27*, 1153–1167. [[CrossRef](#)]
43. Sathiamurthy, E.; Voris, H.K. Maps of Holocene Sea Level Transgression and Submerged Lakes on the Sunda Shelf. *Nat. Hist. J. Chulalongkorn Univ.* **2006**, *2*, 1–43.
44. Solihuddin, T. A Drowning Sunda Shelf Model during Last Glacial Maximum (LGM) and Holocene: A Review. *Indones. J. Geosci.* **2014**, *1*, 2. [[CrossRef](#)]
45. Indonesian Geospatial Agency (BIG). Observasi Dan Prediksi Pasut Serta Hasil Model Laut. 2020. Available online: <http://tides.big.go.id/> (accessed on 17 November 2020).
46. Indonesian Meteorological, Climatological, and Geophysical Agency (BMKG). Kondisi Wilayah Perairan Indonesia. 2020. Available online: <https://peta-maritim.bmkg.go.id/> (accessed on 17 November 2020).
47. Landa, A. *A La Recherche des Coraux Témoins de L'éruption Volcanique du Samalas en 1257*; Memoire M1 Université Paris 1 Panthéon Sorbonne: Paris, France, 2016.
48. Szczuciński, W.; Kokociński, M.; Rzeszewski, M.; Chagué-Goff, C.; Cachão, M.; Goto, K.; Sugawara, D. Sediment sources and sedimentation processes of 2011 Tohoku-Oki tsunami deposits on the Sendai Plain, Japan—Insights from diatoms, nannoliths and grain size distribution. *Sediment. Geol.* **2012**, *282*, 40–56. [[CrossRef](#)]
49. Chagué-Goff, C.; Niedzielski, P.; Wong, H.K.Y.; Szczuciński, W.; Sugawara, D.; Goff, J. Environmental impact assessment of the 2011 Tohoku-Oki tsunami on the Sendai Plain. *Sediment. Geol.* **2012**, *282*, 175–187. [[CrossRef](#)]
50. Goff, J.; Chagué-Goff, C.; Nichol, S.; Jaffe, B.; Dominey-Howes, D. Progress in paleotsunami research. *Sediment. Geol.* **2012**, *243–244*, 70–88. [[CrossRef](#)]
51. Stuiver, M.; Reimer, P.J.; Reimer, R.W. CALIB 8.2. Available online: <http://calib.org> (accessed on 22 October 2020).
52. Heaton, T.J.; Köhler, P.; Butzin, M.; Bard, E.; Reimer, R.W.; Austin, W.E.N.; Ramsey, C.B.; Grootes, P.M.; Hughen, K.A.; Kromer, B.; et al. Marine20—The Marine Radiocarbon Age Calibration Curve (0–55,000 cal BP). *Radiocarbon* **2020**, *62*, 779–820. [[CrossRef](#)]
53. Allen, G. *Marine Life of the Pacific and Indian Oceans*; Tuttle Publishing: North Clarendon, UK, 2001; p. 21.
54. Wassmer, P.; Gomez, C. Development of the AMS Method for Unconsolidated Sediments, Application to Tsunami deposits. *Geomorphol. Relief Process. Environ.* **2011**, *3*, 279–290. [[CrossRef](#)]
55. Wassmer, P.; Schneider, J.L.; Fonfrère, A.; Lavigne, F.; Paris, R.; Gomez, C. Use of Anisotropy of Magnetic Susceptibility (AMS) in the study of tsunami deposits: Application to the 2004 deposits on the eastern coast of Banda Aceh, North Sumatra, Indonesia. *Mar. Geol.* **2010**, *275*, 255–272. [[CrossRef](#)]
56. Wassmer, P.; Gomez, C.; Iskandaryah, T.Y.W.M.; Lavigne, F.; Sartohadi, J. Contribution of anisotropy of magnetic susceptibility (AMS) to reconstruct flooding characteristics of a 4220 BP tsunami from a thick unconsolidated structureless deposit (Banda Aceh, Sumatra). *Front. Earth Sci.* **2015**, *3*, 40. [[CrossRef](#)]
57. Wassmer, P.; Font, E.; Gomez, C.; Iskandaryah, T.Y.W.M. Magnetic Susceptibility and Anisotropy of Magnetic Susceptibility: Versatile Tools to Decipher Hydrodynamic Characteristics of Past Tsunamis. In *Geological Records of Tsunamis and Other Extreme Waves*; Engel, M., Pilarczyk, J., May, S.M., Brill, D., Garrett, E., Eds.; Chapter 16; Elsevier: Amsterdam, The Netherlands, 2020; pp. 343–363. [[CrossRef](#)]
58. Folk, R.L.; Ward, W.C. A Study in the Significance of Grain-Size Parameters. *J. Sediment. Petrol.* **1957**, *27*, 3–26. [[CrossRef](#)]
59. Blott, S.J.; Pye, K. GRADISTAT: A grain size distribution and statistics package for the analysis of unconsolidated sediments. *Earth Surf. Process. Landf.* **2001**, *26*, 1237–1248. [[CrossRef](#)]
60. Major, J.J. Depositional Processes in Large-Scale Debris-Flow Experiments. *J. Geol.* **1997**, *105*, 345–366. [[CrossRef](#)]
61. Kortekaas, S.; Dawson, A.G. Distinguishing tsunami and storm deposits: An example from Martinhal, SW Portugal. *Sediment. Geol.* **2007**, *200*, 208–221. [[CrossRef](#)]
62. Moore, A.L.; McAdoo, B.G.; Ruffman, A. Landward fining from multiple sources in a sand sheet deposited by the 1929 Grand Banks tsunami, Newfoundland. *Sediment. Geol.* **2007**, *200*, 336–346. [[CrossRef](#)]
63. Dura, T.; Cisternas, M.; Horton, B.P.; Ely, L.L.; Nelson, A.R.; Wesson, R.L.; Pilarczyk, J.E. Coastal evidence for Holocene subduction-zone earthquakes and tsunamis in central Chile. *Quat. Sci. Rev.* **2014**, *113*, 93–111. [[CrossRef](#)]
64. Grauert, M.; Björck, S.; Bondevik, S. Storegga tsunami deposits in a coastal lake on Suouroy, the Faroe Islands. *Boreas* **2001**, *30*, 263–271. [[CrossRef](#)]
65. Donato, S.V.; Reinhardt, E.G.; Boyce, J.I.; Pilarczyk, J.E.; Jupp, B.P. Particle-size distribution of inferred tsunami deposits in Sur Lagoon, Sultanate of Oman. *Mar. Geol.* **2009**, *257*, 54–64. [[CrossRef](#)]
66. Wassmer, P.; Iskandaryah, T.Y.W.M.; Gomez, C.; Lavigne, F.; Hart, D.; Pratomo, I.; Bel, J. When Debris Flows Run Upslope: Tsunami Induced Debris Flows. In *Proceedings of the 8th International Conference on Geomorphology*, Paris, France, 27–31 August 2013.
67. Marris, E. Tsunami damage was enhanced by coral theft. *Nature* **2005**, *436*, 1071. [[CrossRef](#)] [[PubMed](#)]

68. Fernando, H.J.S.; McCulley, J.L.; Mendis, S.G.; Perera, K. Coral poaching worsens tsunami destruction in Sri Lanka. *EOS* **2005**, *86*, 301–304. [[CrossRef](#)]
69. Kunkel, C.M.; Hallberg, R.W.; Oppenheimer, M. Coral reefs reduce tsunami impact in model simulations. *Geophys. Res. Lett.* **2006**, *33*, L23612. [[CrossRef](#)]
70. Baba, T.; Mleczko, R.; Burbidge, D.; Cummins, P.R.; Thio, H.K. The Effect of the Great Barrier Reef on the Propagation of the 2007 Solomon Islands Tsunami Recorded in Northeastern Australia. *Pure Appl. Geophys.* **2008**, *165*, 2003–2018. [[CrossRef](#)]
71. Gabrie, C.; Salvat, B. General Features of French Polynesian Islands and Their Coral Reefs. In Proceedings of the 5th International Coral Reef Congress, Tahiti, French Polynesia, 27 May–1 June 1985.
72. Paulay, G. Productivity plays a major role in determining atoll life and form: Tarawa, Kiribati. In Proceedings of the 8th International Coral Reef Symposium, Balboa, Panama, 24–29 June 1996; Lessios, H.A., MacIntyre, I.G., Eds.; Smithsonian. Trop. Res. Inst.: Balboa, Panama, 1997; Volume 1, pp. 483–488.
73. Takada, A.; Nasution, A.; Rosgandika, M. Eruptive History During the last 10ky for the Caldera-Forming Eruption of Rinjani Volcano. In Proceedings of the Japan Earth and Planetary Science Joint Meeting, Tokyo, Japan, 22–24 October 2003.
74. Nasution, A.; Takada, A.; Rosgandika, M. The volcanic activity of Rinjani, Lombok Island, Indonesia, during the last thousand years, viewed from ¹⁴C datings. In Proceedings of the Convention Bandung 2004, the 33rd Annual Convention & Exhibition, Bandung, Indonesia, 29 November–1 October 2004; pp. 8–15.